Environmental Earth Sciences (2020) 79:343
https://doi.org/10.1007/s12665-020-09088-y

ORIGINAL ARTICLE

Deformation characteristics of granites at different unloading rates after high-temperature treatment

Peng Kang[1,2] · Zhang Jing[1] · Zou Quanle[1] · Song Xiao[1]

Received: 3 August 2019 / Accepted: 20 June 2020 / Published online: 1 July 2020
© Springer-Verlag GmbH Germany, part of Springer Nature 2020

Abstract

Naturally cooled granite specimens pretreated at 800 °C were separately subjected to conventional triaxial compression tests and triaxial confining pressure unloading tests under a constant deviatoric stress. Via these tests, the deformation characteristics of granite at different confining pressure unloading rates were explored. The research results showed that the granite specimens were more easily damaged at an intermediate unloading rate than at a high or low unloading rate. The strain–confining pressure compliance results quantitatively revealed that rock failure during unloading was caused by intense radial deformation and volumetric dilatancy. With the increase in the unloading rate, the strain–confining pressure compliance first increased and then decreased. In the confining pressure unloading process, initially, the elastic modulus of the rocks linearly decreased with the decreasing confining pressure. In the case that the confining pressure was unloaded to the critical point where rock failure occurred, the elastic modulus of the rocks dramatically decreased. Additionally, Poisson's ratio gradually decreased with the reduction in confining pressure. However, approaching the critical point where rock failure occurred during unloading, Poisson's ratio remarkably decreased. Afterwards, Poisson's ratio increased to 0.5 and then remained unchanged until the specimens became damaged.

Keywords Granite · Triaxial confining pressure unloading test · Unloading rate · Deformation characteristics · Deformation parameters

Introduction

Since entering the 21st century, the development of deep underground resources and space (including geothermal utilization, coal mining, oil and gas drilling, and disposal of nuclear wastes) has frequently involved rocks in high-temperature environments (Feng et al. 2012). By taking the disposal of nuclear wastes as an example, nuclear energy is widely used in industrial production and scientific research as an efficient clean energy source, resulting in a large number of different types of radioactive nuclear waste. Researchers are also exploring methods for safely and permanently disposing nuclear wastes while utilizing nuclear energy. At present, people generally prefer to utilize deep rock chambers (e.g., in granite) buried 500–1000 m underground as permanent repositories. Numerous tests and studies have verified that radioactive elements in nuclear wastes release a great amount of heat during disintegration. Generally, this heat will increase he temperature of the rocks surrounding the repository, and the physical and mechanical properties of rocks change at a high temperature. For example, Aversa and Evangelista (1998), Chaki et al. (2008), Yu et al. (2015), and Popov et al. (016) suggested that the elastic modulus and mechanical strength of rocks can decrease due to the influence of high temperatures. The change in the physical and mechanical properties of rocks likely results in serious problems related to the deformation and stability of the geological bodies around the nuclear waste repositories (Hashemi et al. 2015). Therefore, exploring the strength and deformation characteristics of granites treated at a high temperature has been an important topic for investigating the long-term stability and safety of the rocks surrounding

✉ Peng Kang
pengkang@cqu.edu.cn

✉ Zou Quanle
quanlezou2016@cqu.edu.com

[1] State Key Laboratory of Coal Mine Disaster Dynamics and Control, College of Resources and Environmental Science, Chongqing University, Chongqing 400044, China

[2] State Key Laboratory of Coal Resources and Safe Mining (CUMT), Xuzhou 221006, China

nuclear waste repositories. Vázquez et al. (2015), Nguyen et al. (2011), Zhang et al. (2016), and Yin et al. (2016) carried out various experiments on the mechanical properties of rocks at a high temperature. On this basis, they found that various mechanical properties (including the elastic modulus, failure strength, and deformation characteristics) of rocks are all affected by temperature. To investigate changes in the microstructure morphologies of granite, individual crystals, and the porosity of rocks at a high temperature, Zhang et al. (Zhang et al. 2018) performed a series of experiments after heating and rapid cooling of granite samples and found that as the temperature increased, the elastic modulus and cohesion of the granite decreased significantly and that the rate of decrease became slower as the confining pressure increased. Lönnqvist and Hökmark (2016) and Yao et al. (2016) revealed that changing temperatures result in a complex stress distribution in crystalline rocks due to thermal expansion of the minerals. After summarizing the relationship between the strength and temperature of rocks, Wong (1982) suggested that the strength of most rocks decreases with increasing temperature and that the reduction trend is related to the type of rock. Heueckel et al. (1994) attained the deformation mechanism of rocks by using clays as representative materials. Chen et al. (2012) and Liu and Xu (2014) investigated the physical and mechanical properties of granites under uniaxial compression after conducting thermal treatments at different temperatures. Du et al. (2004) carried out a uniaxial test to explore the mechanical properties of granites after being treated at different temperatures. Fang et al. (2016) analyzed the splitting failure modes of granites after being treated at different temperatures by conducting a Brazilian disc test on granites subjected to high-temperature treatment. Zhu et al. (2018) revealed the change in the physical and mechanical properties of granites with temperature after the high-temperature granites were cooled with water. By carrying out conventional triaxial tests on granites treated at high temperatures, Xu et al. (2014) presented that temperature is the primary factor influencing the mechanical properties of granites. Numerous remarkable achievements have been made on the mechanical properties of rocks treated at high temperatures. However, a majority of studies are conducted under uniaxial compression or conventional triaxial compression conditions, mainly aiming at the mechanical properties of high-temperature rocks under these loading conditions.

The reduction in the confining pressure of rocks as a result of the excavation of a rock mass is the key cause of the failure of rocks in deep underground engineering. In the aforementioned process, rocks are mainly under an unloading stress path and show an essential difference in mechanical properties compared to those of rock masses under loading conditions (Wu and Zhang 2004; Xie and He 2004; Peng et al. 2019a, b). Li et al. (2014) investigated the influence of the stress path on the unloading response during excavation. Chen et al. (2018) suggested that with the decrease in deformation modulus during the confining pressure unloading process, the damage variable gradually increases, indicating that confining pressure unloading is a process of damage accumulation and strength degradation. Qiu et al. (2012) carried out a triaxial confining pressure unloading test (TUTCP) on deeply buried marble under different initial damage levels and unloading paths and further proposed new parameters for describing the mechanics of a rock mass under unloading conditions. Li et al. (2019) conducted a series of triaxial prepeak unloading limiting pressure tests at different initial limiting pressure levels. Based on the results of the unloading testing, the effect of the unloading stress path on the dilatancy characteristics of sandstone was analyzed, and the unloading stress was summarized. The variation law of the dilatancy angle under the path was established by a linear fitting method using confining pressure and postpeak plastic shear strain as the independent variables. Lu et al. (2009) described the degradation law of the mechanical parameters of granites during unloading. The above achievements mainly reveal the mechanical properties and failure characteristics of rocks under different initial unloading levels. Furthermore, a constitutive model for rock failure under unloading conditions is established. However, research on the mechanical properties of rocks undergoing thermal damage under unloading conditions is scarce. Li et al. (2011) and Cai et al. (2015) separately presented the mechanical properties and deformation and failure characteristics of sandstones and granites under triaxial unloading conditions treated at high temperatures. In the confining pressure unloading testing of rocks, the unloading rate of the confining pressure also shows a certain influence on the change in the mechanical properties of the rocks. By contrast, research on the control of the unloading rate on the deformation characteristics of rocks subjected to thermal treatment during the unloading of confining pressure is scarcely reported.

Thus, unlike the currently available research using uniaxial compression or conventional triaxial compression tests to study the mechanical properties of granite subjected to high temperature, this paper mainly uses triaxial unloading and confining pressure to treat granite samples subjected to 800 °C and then naturally cooled. Triaxial unloading mechanical tests with different unloading rates were carried out, and the unloading method was used to maintain a constant deflection stress. By changing the unloading rate of the confining pressure, the influence of the unloading conditions on the mechanical properties of the granites that underwent high-temperature treatment was explored, and the influence of different confining pressure unloading rates on the mechanical properties of granites subjected to thermal damage was analyzed. The research results provide theoretical

guidance for revealing the deformation mechanism and formulating prevention measures for disasters induced by unloading in deep underground rock engineering projects in high-temperature conditions.

Experimental materials and scheme

Rock specimen preparation

The rock specimens were taken from an intact horizontally oriented granite block buried 930 m underground in the Xincheng gold ore (Xincheng village, Jincheng Town, Laizhou, Shandong Province, China). To ensure the homogeneity and comparability of rock specimens, the rock specimens were collected from adjacent positions in the same large intact rock block. After eliminating the rock specimens with significant defects (including joints or cracks), the rest of the rock specimens were cored, cut, ground, and processed into cylindrical specimens 100 mm in height and 50 mm in diameter in the laboratory. The machining accuracy of such specimens should reach the standard in *Code for Rock Tests of Hydroelectric and Water Conservancy Engineering* (SL264-2001). The unevenness of the end face of the specimens was within ± 0.02 mm, and the end face was perpendicular to the axis of the specimens, with an allowable deviation no greater than 0.25°. The specimens were heated by employing an SRX2-4-10 high-temperature box-type electric resistance furnace with a rated power, voltage, and temperature of 2.5 kW, 220 V, and 1000 °C, respectively, in which the electric furnace heating wire was used for heating, as shown in Fig. 1. The rock specimens were heated to 800 °C at a rate of 10 °C/min and then kept at 800 °C for 6 h so that they were uniformly heated. Then, the specimens were removed from the furnace after being naturally cooled to room temperature. The basic parameters of the rock specimens used for the test are displayed in Table 1.

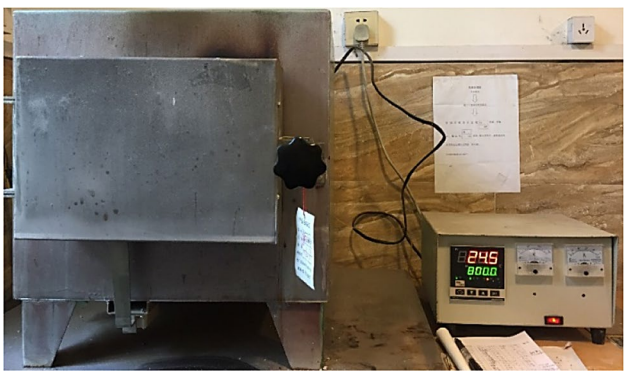

Fig. 1 SRX2-4-10 high-temperature box-type electric resistance furnace

Table 1 Basic parameters of the rock specimens

Serial number of rock specimens	Diameter/mm	Height/mm	Mass/g	Density/(g cm^{-3})
A	50.18	100.00	523.82	2.65
B	49.16	99.56	503.30	2.66
C	49.88	99.64	521.48	2.68
D	49.98	99.68	519.64	2.66

After being subjected to high-temperature treatment, the color of the rock specimens changed from grayish white to white, and images of rock specimens before and after being subjected to high-temperature treatment are shown in Fig. 2.

Test equipment

An RTX-3000 high-temperature and high-pressure triaxial testing machine for rocks produced by the GCTS Corporation in the United States was used in this work. The maximum axial load that can be applied by the system was 3000 kN. The circumferential deformation of rock specimens during the test was measured by using a chain-linked circumferential extensometer, and the chain was installed around the middle part of the specimens. The axial deformation of the rock specimens was measured by utilizing two axial extensometers, as shown in Fig. 3. During the experimentation, loading and unloading tests were conducted by controlling the deviatoric stress, that is, the deviatoric stress (σ_1–σ_3) remained unchanged during the test. In the triaxial loading stage, the displacement was controlled during the loading, with an axial pressure loading rate of 0.02 mm/min. In the unloading stage, the stress was controlled. The test was controlled via full-digital computer control, and the test data were automatically collected.

Test scheme

In the confining pressure unloading process, different stress paths arise. According to the change in deviatoric stress in the confining pressure unloading process, the stress paths in the unloading process of the confining pressure of rocks can be divided into the following kinds, as shown in Fig. 4. In the figure, OA denotes the conventional triaxial compression test, that is, when the keeping confining pressure is kept constant, the axial pressure is constantly applied until the rock specimen becomes damaged (the imaginary line in the figure refers to the assumed nonlinear strength criterion); OB denotes the increase in axial pressure while unloading the confining pressure until the rock specimen becomes damaged; OC represents unloading the confining pressure while maintaining the axial pressure until the rock specimen becomes damaged; OD refers to unloading the

(a) (b)

Fig. 2 Granite specimens before and after high-temperature treatment; **a** granite specimens before high-temperature treatment; **b** granite specimens after high-temperature treatment

Fig. 3 RTX-3000 triaxial testing machine system for rocks

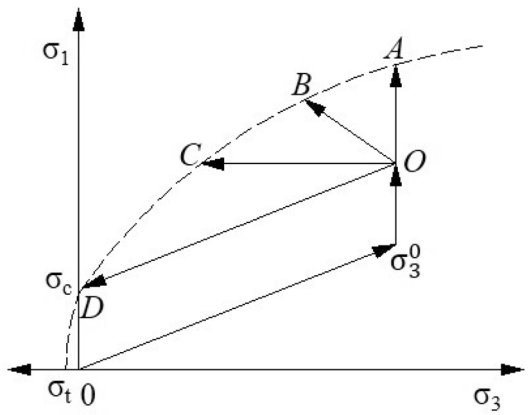

Fig. 4 Different stress paths of unloading confining pressure

confining pressure until the rock specimen becomes damaged while maintaining the deviatoric stress. Unloading the confining pressure while maintaining the deviatoric stress is equivalent to unloading the axial pressure and confining pressure. In previous studies, a majority of scholars have carried out research aimed at stress paths OB and OC. By contrast, there are few studies in which the deviatoric stress was held constant (path OD). Deng et al. (2017) investigated the relationship between the characteristics of sandstones during unloading and pore water pressure in the case that the deviatoric stress remained unchanged. Under different loading and unloading stress paths, different test laws can be attained, which is also one of the important reasons why the laws obtained through unloading tests vary at present (Qiu et al. 2012). For the aforementioned three stress paths, the main distinction lies in the change in axial pressure during unloading of the confining pressure. At present, research on unloading tests of confining pressure while maintaining the deviatoric stress is rarely reported. Therefore, the influence of the confining pressure unloading rate on the mechanical properties of rocks under unloading conditions was explored under the stress path (OD in Fig. 4) of unloading the confining pressure while maintaining the deviatoric stress.

The test scheme is described as follows: first, by conducting a conventional triaxial tests with a confining pressure of 10 MPa, the peak strengths of the naturally cooled specimens treated at 800 °C were determined. Afterwards, tests were carried out to detect the mechanical properties of the rocks at different unloading rates, and the design scheme is displayed in Table 2. The steps of the confining pressure unloading testing of the rock specimens at different unloading rates are as follows: (1) the confining pressure and axial pressure were loaded to the preset value of 10 MPa by controlling the stress. During loading, the rates of increase in the confining pressure and axial pressure were both maintained at 2 MPa/min. (2) After the confining pressure reached the

Table 2 Test scheme with different confining pressure unloading rates

Number	Axial pressure/MPa	Confining pressure/MPa	Confining pressure unloading rate/(kPa s^{-1})
A	125	10	5.0
B	125	10	7.5
C	125	10	9.5
D	125	10	11.5

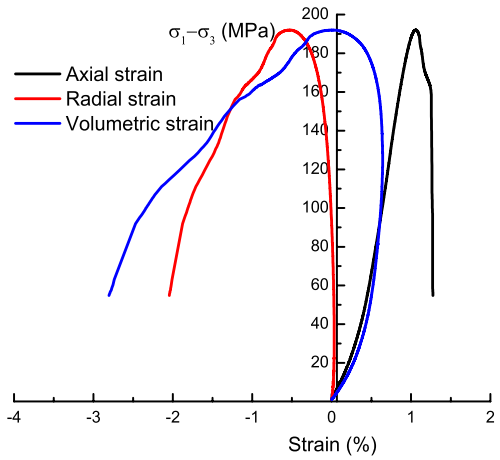

Fig. 5 The deviatoric stress–strain curves of granites undergoing high-temperature treatment in the conventional triaxial compression test

preset value, the axial load was continuously applied at the loading rate of 0.02 mm/min through displacement control until reaching 60% of the ultimate bearing capacity of the rock specimens under the confining pressure. In this case, the stress on the rock specimens stabilized for 5 min. (3) When the deviatoric stress remained unchanged, the confining pressure of the rock specimens was unloaded at different unloading rates. (4) The confining pressure unloading immediately ceased after the rock specimens were subjected to a dramatic stress drop. In this context, the rock specimens were completely damaged, and the test was ended.

Results

Characteristics of the deviatoric stress–strain curves under conventional triaxial loading conditions

Figure 5 shows the deviatoric stress–strain curves of the rock specimens under conventional triaxial loading conditions under a confining pressure of 10 MPa. The confining pressure of rocks was first loaded to the preset value of 10 MPa under hydrostatic pressure conditions. Afterwards, in the case of maintaining the confining pressure, the axial load was continuously applied until the rock specimen became damaged. It can be seen from the figure that under loading conditions with a constant confining pressure, the granite specimens treated at high temperatures exhibited a short compaction stage of axial strain. This occurred because at a high temperature, some of the water in the rocks evaporated, resulting in air expansion. Moreover, the addition of the confining pressure led to the compaction or narrowing of the fractures in the rocks. Therefore, the compactness of the rock was increased. Before the axial strain reached the peak strain, the elastic stage was significant, and the stress was approximately linearly correlated with the strain. In this stage, the growth rates of the radial strain and volumetric strain decreased. When the axial strain reached its maximum, the postpeak stress rapidly dropped, and the rock specimen underwent brittle failure.

Characteristics of the deviatoric stress–strain curves at different confining pressure unloading rates

The stress under which the volume recovered was taken as the initial axial stress during the confining pressure unloading test. According to the stress–strain curves from the conventional triaxial compression test in Fig. 5, the rock specimens started to recover from the volumetric strain when reaching approximately 60% of the peak strength. In this case, the deviatoric stress was 115.2 MPa. For the convenience of operation, the deviatoric stress was 115 MPa in the test. Thus, the initial axial stress during the confining pressure unloading test was approximately 60% of the peak strength from the triaxial compression test.

Figure 6 shows the deviatoric stress–strain curves of naturally cooled granites subjected to high-temperature treatment under TUTCP at different unloading rates. As shown in the figure, at different confining pressure unloading rates, the deviatoric stress–strain curves of the rocks treated at high temperatures showed similar change characteristics. According to the change in the deviatoric stress–strain curve, the following three stages can be identified:

1. Loading stage of confining pressure: The strain greatly increased in the stage. When the confining pressure increased from 0 to 10 MPa, the circumferential strain continuously increased, and the deviatoric stress–strain curve was concave. Moreover, the rate of increase in the strain decreased, that is, the rate of increase in the circumferential strain was high in the initial confining pressure loading stage. The rate of increase in the circumferential strain decreased as the confining pressure approached 10 MPa. In this stage, the change trends of axial strain and volumetric strain were the same as that of circumferential strain, all showing a reduction in the

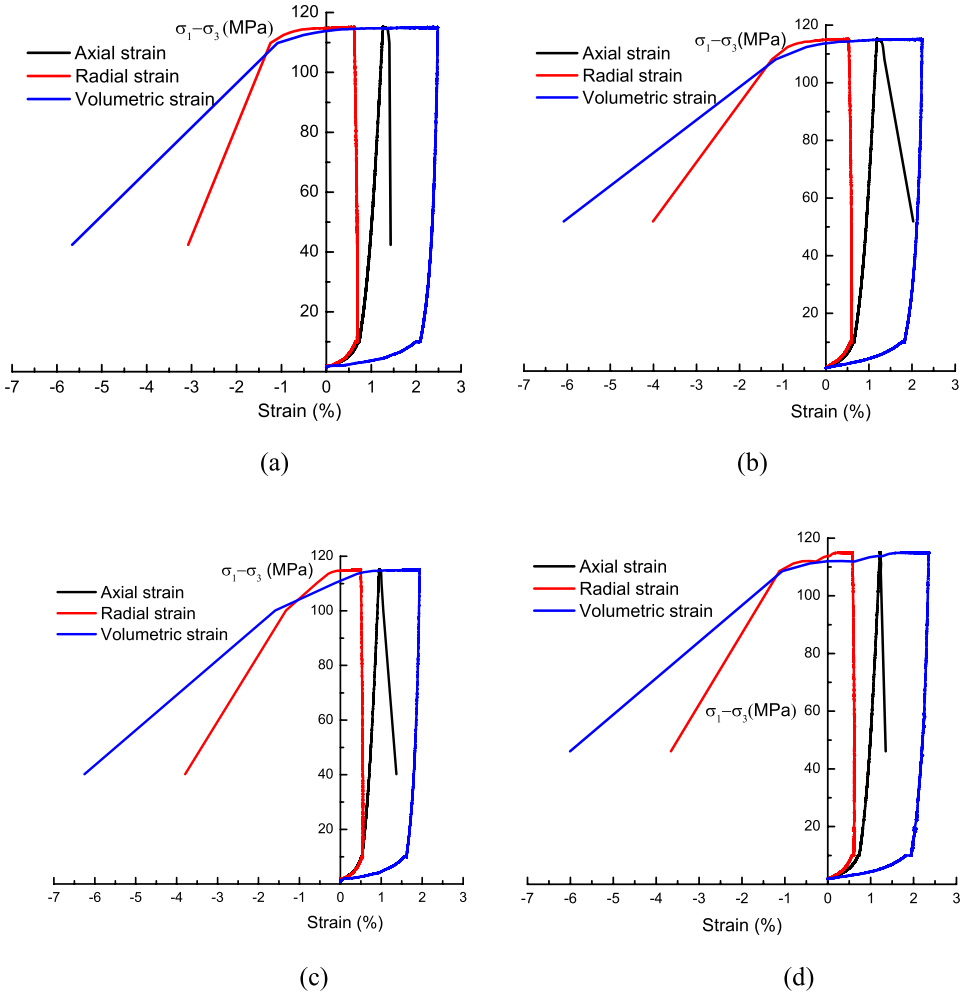

Fig. 6 Deviatoric stress–strain curves at different confining pressure unloading rates. **a** Unloading confining pressure at 5.0 kPa/s. **b** Unloading confining pressure at 7.5 kPa/s. **c** Unloading confining pressure at 9.5 kPa/s. **d** Unloading confining pressure at 11.5 kPa/s

rate of increase in the strain. The reason for this consistency was that the fractures that formed in damaged granites due to being heated were compacted or narrowed in the initial loading stage, thus resulting in the increase in the axial and radial strains. Among the three groups of tests, the radial strains exhibited an insignificant difference when the confining pressure increased to 10 MPa.

2. Loading stage of confining pressure: On the condition that the confining pressure was kept at 10 MPa and the axial pressure was continuously loaded to 60% of the peak strength during the triaxial compression test, the axial strain continuously increased while the radial strain gradually decreased, with an insignificant variation. Figure 6 shows that the deviatoric stress–strain curve of the granites was approximately linear and that these rocks underwent significant elastic deformation in this stage. In this stage, the rocks had not yet been subjected to nonrecoverable deformation.
3. Unloading stage of confining pressure: When the deviatoric stress was held constant and the confining pressure was gradually unloaded, the yield stage of the rocks was significant, and the deviatoric stress–strain curve was approximately horizontal. In this case, the axial deformation occurred relatively slowly, while the radial deformation rapidly increased. As a result, the rock specimens were subjected to nonrecoverable radial plastic deformation. The primary cracks in the specimens propagated and cut through the sample or new cracks initiated with the reduction in confining pressure, thus eventually generating through-going cracks that enabled the overall failure of the rock specimens. In this process, the volume of the rocks expanded and the deformation of the rocks dramatically increased after the confining pressure was reduced to a certain level. In this context, an obvious stress drop can be identified.

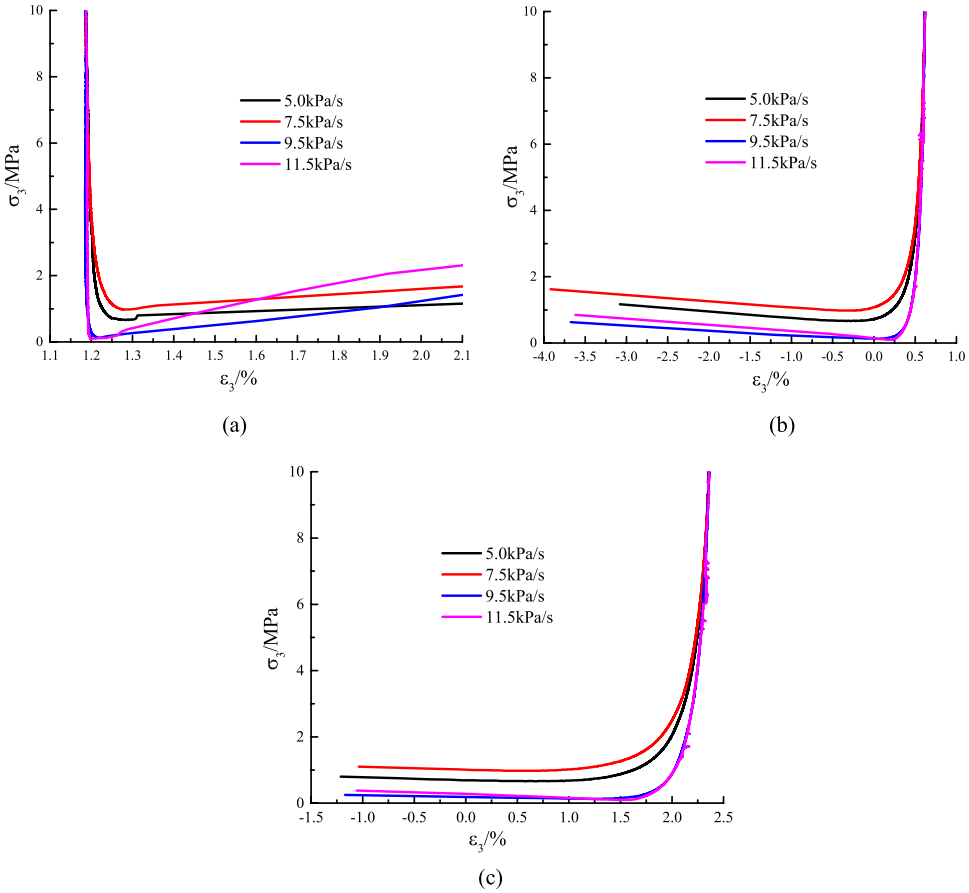

Fig. 7 Relations between the confining pressure and various strains in the confining pressure unloading process of granites subjected to high-temperature treatment. **a** Relationship between confining pressure and axial strain. **b** Relationship between confining pressure and radial strain. **c** Relationship between confining pressure and volumetric strain

Discussion

The influence of unloading rate on the confining pressure–strain relationship

Figure 7 shows the relationship between confining pressure and strain in the confining pressure unloading process of the granites. During the confining pressure unloading test at different unloading rates, the time when the confining pressure was completely unloaded varied, the strains in the rock specimens at the same time also varied. To conveniently analyze the trend of the change in the confining pressure with strain, the confining pressure–strain relationship curves in the unloading stage for the four groups of tests were normalized. Although the strains at the initial unloading points were the same, this normalization did not affect the trends of the changes in the confining pressure with strain at different unloading rates. As shown in Fig. 7a, in the initial confining pressure unloading stage (to 50% of the initial confining pressure), the axial deformations at different unloading rates remained nearly unchanged. This result indicated that in the confining pressure unloading process, the unloading of confining pressure insignificantly influenced the axial deformation when the deviatoric stress remained unchanged. According to Fig. 6, the elastic modulus of the specimens was maximized. Additionally, under the condition that the unloading rate was 7.5 kPa/s, the rock specimens underwent nonrecoverable plastic deformation before failure. At large unloading rates (9.5 and 11.5 kPa/s), no significant plastic deformation was observed before the failure of the rock specimens. This result indicated that the rocks exhibited remarkable brittle failure at a high confining pressure unloading rate. It can be seen from Fig. 7 that during the failure of the rock specimens, the confining pressure was unloaded the least amount (the lowest confining pressure was 0.97 MPa) at the unloading rate of 7.5 kPa/s, followed by the unloading rates of 5.0 and 9.5 kPa/s, at which the lowest confining pressures were 0.75 and 0.14 MPa, respectively. At the unloading rate of 11.5 kPa/s, the confining pressure was nearly completely unloaded. In this case, the lowest confining pressure was 0.1 MPa.

Figure 7b, c shows that in the initial confining pressure unloading stage, the radial and volumetric deformations insignificantly increased. In this context, the rock specimens were still in a linear-elastic stage. However, with a further reduction in the confining pressure, the radial and volumetric deformations rapidly increased, no longer linearly increasing with the confining pressure. This result indicated that

the rock specimens were subjected to nonrecoverable plastic deformation; cracks in the rock specimens gradually initiated, propagated, and cut through, ultimately leading to the failure of the rock specimens. It can be seen from the figures that at different unloading rates, the change in the radial strain with the confining pressure was similar to that of the volumetric strain with the confining pressure. However, the curve at the unloading rate of 7.5 kPa/s plotted above the other curves, and the decrease in the confining pressure at this unloading rate (7.5 kPa/s) was lower than those at the unloading rates of 5.0, 9.5, and 11.5 kPa/s during the failure of the rock specimens. This finding implied that the rocks were more easily damaged when the confining pressure was unloaded at a rate of 7.5 kPa/s.

Figure 7 shows that the decrease in the confining pressure was the lowest at the unloading rate of 7.5 kPa/s. Compared with the other three confining pressure unloading rates, at this unloading rate (7.5 kPa/s), the rock specimens were most easily damaged. This result indicated that both low and high confining pressure unloading rates can inhibit the failure of rock specimens in the confining pressure unloading process. An intermediate confining pressure unloading rate can promote the deformation of rock specimens in this process.

The influence of unloading rate on strain–confining pressure compliance

To analyze the deformation process of rocks in the unloading process, the strain–confining pressure compliance proposed by Qiu et al. (2010) was introduced. The strain–confining pressure compliance $\Delta\dot{\varepsilon}_i$ refers to the ratio of incremental strain induced by the unloading of the confining pressure to the reduction in the confining pressure between the initial point of confining pressure unloading and the stress drop, as expressed as follows:

$$\Delta\dot{\varepsilon}_i = \frac{\Delta\varepsilon_i}{\Delta\sigma_3}, \tag{1}$$

where $\Delta\dot{\varepsilon}_i$ ($i = 1, 3, v$) represent the incremental axial, circumferential, and volumetric strains, respectively. The strain–confining pressure compliance $\Delta\dot{\varepsilon}_i$ is a physical quantity displaying the rates of increase in the various deformations when unloading a unit of confining pressure. It favorably reflects the influence of changing the confining pressure on the deformation in the confining pressure unloading process and reveals the speed of the response of the internal structure of rocks to the change in stress state. The larger the strain–confining pressure compliance $\Delta\dot{\varepsilon}_i$ was, the more sensitive the deformation in a certain direction to the reduction in confining pressure.

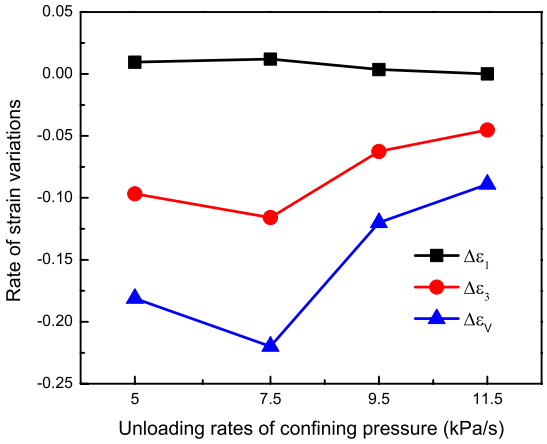

Fig. 8 Relationship between the strain–confining pressure compliance of granites and the unloading rate

According to the test result, the axial strain–, radial strain–, and volumetric strain–confining pressure compliances between the starting and end points in the confining pressure unloading process at different rates are shown in Fig. 8. By comparing the three curves in Fig. 8, it can be found that in the confining pressure unloading process of granites, the confining pressure unloading rate exhibited a significant influence on the axial, radial, and volumetric strains in the rocks. Additionally, compared with radial strain– and volumetric strain–confining pressure compliances, the axial strain–confining pressure compliance was always lower. This implied that in the whole confining pressure unloading process of rocks, the influence of the unloading rate was the lowest on the axial deformation. In contrast, the radial and volumetric deformations were more sensitive than the axial deformation was to the changing confining pressure. According to the changes in the axial strain–confining pressure compliance ($\Delta\dot{\varepsilon}_1$) at different confining pressure unloading rates shown in Fig. 8, the confining pressure unloading rate insignificantly affected the axial deformation. The axial strain–confining pressure compliance curve changed gently with increasing unloading rate. Additionally, with the increase in the unloading rate, the axial strain–confining pressure compliance first increased and then decreased. The maximum axial strain–confining pressure compliance (1.20%) was observed for the unloading rate of 7.5 kPa/s. This result indicated that both a high and a low confining pressure unloading rate showed an inhibitory effect on axial deformation. With increasing unloading rate, the axial strain–confining pressure compliance gradually decreased. Moreover, the rate of decrease in the axial strain–confining pressure compliances when the unloading rate increased from 7.5 to 9.5 kPa/s was larger than that when the unloading rate increased from 9.5 to 11.5 kPa/s. This finding implied that the inhibition effect of a large confining pressure unloading rate on the axial deformation was weakened by increasing the unloading rate.

In Fig. 8, at different unloading rates, the trends of the change in the radial strain–confining pressure compliance ($\Delta\dot{\varepsilon}_3$) with the unloading rate conformed to those of the volumetric strain–confining pressure compliance ($\Delta\dot{\varepsilon}_v$). With the increase in the confining pressure unloading rate, the radial strain– and volumetric strain–confining pressure compliances both first significantly increased and then decreased. At the unloading rate of 7.5 kPa/s, the radial and volumetric deformations were more sensitive to changing confining pressure, with variations in the radial strain– and volumetric strain–confining pressure compliances of 11.60 and 21.99%, respectively. With an increasing confining pressure unloading rate, the sensitivity weakened, implying that both a high and a low unloading rate showed an inhibition effect on the radial and volumetric deformations. When the unloading rate of the confining pressure increased from 7.5 to 9.5 kPa/s, the variations in the radial strain– and volumetric strain–confining pressure compliances were 5.35 and 9.98%, respectively. In contrast, when the unloading rate increased by the same value from 9.5 to 11.5 kPa/s, the variations in the corresponding radial strain– and volumetric strain–confining pressure compliances were 1.73 and 3.10%, respectively. This further validated that the inhibition effect of a high unloading rate on the radial and volumetric deformations decreased with increasing unloading rate.

The influence of the unloading rate on the deformation parameters

In rock mechanics, the elastic modulus is generally calculated according to the elastic stage results of uniaxial or triaxial compression tests. However, when calculating deformation parameters for the confining pressure unloading process, it is necessary to comprehensively consider the influences of the stresses and strains in different directions. According to the generalized Hooke law, it is supposed that each stress and deformation point along the stress–strain curve of a rock in the process of rock failure caused by unloading conforms to the generalized Hook law. By applying this assumption, Huang and Huang (2010) solved the deformation parameters in the deformation and failure process of rocks due to unloading to appropriately grasp the weakening law of the deformation parameter during unloading. The formula for calculating the deformation parameters based on the generalized Hook law is expressed as follows:

$$\left.\begin{array}{c} E = \left(\sigma_1 - 2\mu\sigma_3\right)/\varepsilon_1 \\ \mu = \left(B\sigma_1 - \sigma_3\right)/\left[\sigma_3(2B-1) - \sigma_1\right] \\ B = \varepsilon_3/\varepsilon_1 \end{array}\right\}. \quad (2)$$

Figures 9 and 10 show the changes in the deformation modulus E and Poisson's ratio μ, respectively, with the unloading rate for four unloading rates (5.0, 7.5, 9.5, and 11.5 kPa/s).

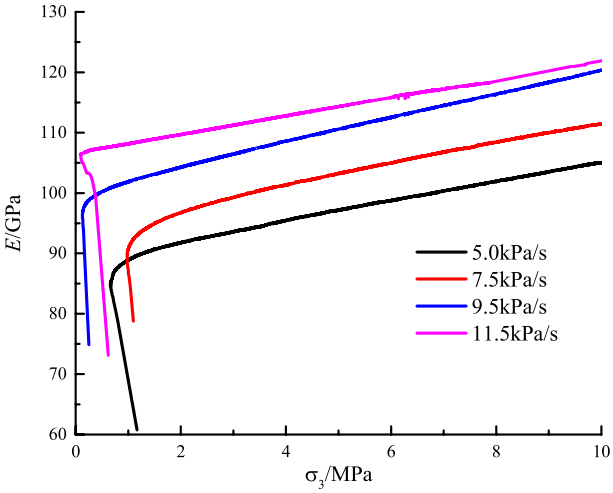

Fig. 9 The characteristics of the change in the deformation modulus in the confining pressure unloading process

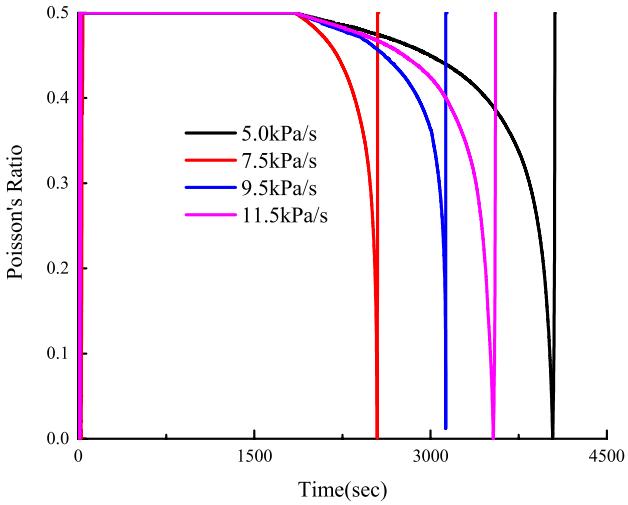

Fig. 10 The characteristics of the change in Poisson's ratio in the confining pressure unloading process

As shown in Fig. 9, the initial elastic modulus in the unloading process increased with the unloading rate. The elastic modulus of the rocks basically showed the same change trend at different confining pressures unloading rates, suggesting that the deformation parameters linearly decreased with decreasing confining pressure in the initial unloading stage. When the confining pressure was unloaded to the point where rock failure occurred, the deformation parameters dramatically decreased. By comparing the change curves of the deformation parameters at different unloading rates shown in Fig. 9, it can be found that the reduction in the deformation parameters during confining

pressure unloading at the unloading rate of 7.5 kPa/s was 70% of the initial deformation modulus. The reductions were greater than 70% at the other three unloading rates, which indicated that rock failure was more likely to occur at the confining pressure unloading rate of 7.5 kPa/s.

It can be seen from Fig. 10 that in the confining pressure unloading process under the condition of an unchanged deviatoric stress, the Poisson's ratio of the rock specimens slightly varied for some time after unloading, showing a decreasing trend. However, when the confining pressure was unloaded to the critical point where rock failure was about to happen, the Poisson's ratio of the rock specimens dramatically decreased, with an exponential change. Afterwards, Poisson's ratio increased and stabilized at 0.5 until rock failure occurred. As shown in Fig. 6, the Poisson's ratio results showed such a change because in the confining pressure unloading process for the case of an unchanged deviatoric stress, the axial deformation slowly changed while the radial deformation constantly varied from a positive strain to a negative strain. Moreover, the Poisson's ratio response reflected the effect of the radial strain in the axial direction. Therefore, in the test process, the dynamic Poisson's ratio recorded by the testing machine constantly decreased with a decreasing confining pressure, and Poisson's ratio rapidly increased to 0.5 after the specimens were damaged. It can be seen from the figure that the larger the unloading rate was, the more rapid the change in Poisson's ratio. The reason why the deformation parameters of the rocks exhibited such a change can be summarized as follows: due to the high-temperature treatment, the microcracks in the rocks dilated, and the volume of the dilatated pores remained unchanged during the cooling process. Under the loading effect, the dilatated pores absorbed the radial deformation generated under the axial load to some extent so that Poisson's ratio decreased macroscopically.

Conclusions

In this paper, the naturally cooled granite specimens treated at 800 °C were separately subjected to conventional triaxial compression test and TUTCP under the condition of an unchanged deviatoric stress by utilizing the RTX-3000 high-temperature and high-pressure triaxial testing machine for rocks. On this basis, the deformation characteristics of granites were explored at different unloading rates of confining pressures. Furthermore, the following conclusions were drawn:

1. The variations in the deformation of all the specimens present similar tendencies. The radial and volumetric deformations insignificantly increased at the initial confining pressure unloading stage. With the gradual reduction in confining pressure, the increments in radial and volumetric deformations rapidly increased, causing nonrecoverable plastic deformation. The reduction in confining pressure at an intermediate unloading rate was lower than those at lower and higher confining pressure unloading rates, indicating that an intermediate unloading rate can promote the deformation of rocks.
2. The strain–confining pressure compliance was used to reflect the impact of the change in confining pressure on the deformation during the unloading process. The strain–confining pressure compliance of the granite specimens first increased and then decreased with increasing confining pressure unloading rate. Compared with an intermediate confining pressure unloading rate, both a lower and a higher unloading rate showed an inhibitory effect on the deformation of rocks. The inhibition effect of a higher unloading rate on the radial and volumetric deformations weakened with the increase in the unloading rate. Additionally, compared with the axial strain, the radial and volumetric deformations were more sensitive to the change in confining pressure.
3. The effect of different unloading rates on the deformation parameters of granite was elaborated in this paper. The trends of the change in the elastic modulus of the rocks were basically the same at different confining pressure unloading rates, and the reduction in the deformation parameter was the lowest at the confining pressure unloading rate of 7.5 kPa/s. Rock failure was more likely to occur at this confining pressure unloading rate than at the other tested rates. Poisson's ratio gradually decreased with decreasing confining pressure. The Poisson's ratio of the rock specimens was insignificantly changed in the initial unloading stage, while it was exponentially reduced when rock failure was about to occur during later unloading. This trend continued until the rock specimens were damaged; then, Poisson's ratio suddenly rose and stabilized at 0.5.

Acknowledgements This work was funded by the State Key Research Development Program of China (2017YFC0804206), National Natural Science Foundation of China (51974043, 51704046, and 51774058), the Chongqing Basic Research and Frontier Exploration Project (cstc2018jcyjA3320), and the Research Fund of the State Key Laboratory of Coal Resources and Safe Mining, CUMT (SKLCRSM18KF025), which are gratefully acknowledged. The authors also thank the editor and anonymous reviewers for their valuable advice.

Compliance with ethical standards

Data availability statement Some or all of the data, models, or code generated or used during the study are available from the corresponding author by request.

References

Aversa S, Evangelista A (1998) The mechanical behaviour of a pyroclastic rock: yield strength and "destructuration" effects. Rock Mech Rock Eng 31(1):25–42

Cai YY, Luo CH, Yu J, Zhang LM (2015) Experimental study on mechanical properties of thermal-damage granite rock under triaxial unloading confining pressure. Chin J Geotech Eng 37(7):1173–1180

Chaki S, Takarli M, Agbodjan WP (2008) Influence of thermal damage on physical properties of a granite rock: porosity, permeability and ultrasonic wave evolutions. Constr Build Mater 22(7):1456–1461

Chen YL, Ni J, Shao W, Azzam R (2012) Experimental study on the influence of temperature on the mechanical properties of granite under uni-axial compression and fatigue loading. Int J Rock Mech Min 56:62–66

Chen X, Tang CA, Yu J, Zhou JF, Cai YY (2018) Experimental investigation on deformation characteristics and permeability evolution of rock under confining pressure unloading conditions. J Central South Univ 25(8):1987–2001

Deng HF, Wang Z, Li JL, Jiang Q, Zhang HB (2017) Effect of unloading rate and pore water pressure on mechanical properties of sandstone. Chin J Geotech Eng 39(11):1976–1983

Du SJ, Liu H, Zhi HT, Chen HH (2004) Testing study on mechanical properties of post-high- temperature granite. Chin J Rock Mech Eng 23(14):2359–2364

Fang XY, Xu JY, Liu S, Wang P (2016) Research on splitting-tensile tests and thermal damage of granite under post-high temperature. Chin J Rock Mech Eng 35(S1):2687–2694

Feng ZJ, Zhao YS, Zhou AC, Zhang N (2012) Development program of hot dry rock geothermal resource in the Yangbajing Basin of China. Renew Energy 39(1):490–495

Hashemi SS, Melkoumian N, Taheri A (2015) A borehole stability study by newly designed laboratory tests on thick-walled hollow cylinders. J Rock Mech Geotech Eng 7(5):519–531

Heueckel T, Peano A, Pellegrini R (1994) A constitute law for thermoplastic behavior of rocks:an analogy with clays. Surv Geophys 15(5):643–671

Huang RQ, Huang D (2010) Experimental research on affection laws of unloading rates on mechanical properties of Jinping marble under high geostress. Chin J Rock Mech Eng 29(1):21–33

Li JL, Chen X, Dang L, Dong YH, Cheng Z, Guo J (2011) Triaxial unloading test of sandstone after high temperature. Chin J Rock Mech Eng 30(8):1587–1595

Li XB, Cao WZ, Zhou ZL, Zhou Y (2014) Influence of stress path on excavation unloading response. Tunnel Undergr Space Technol 42:237–246

Li JP, Gao L, Mu HS (2019) Dilatancy characteristics of sandstone and its function of dilatancy angle under high confining pressure and unloading conditions. Rock Soil Mech 40(6):2119–2126

Liu S, Xu JY (2014) Mechanical properties of Qinling biotite granite after high temperature treatment. Int J Rock Mech Min 71:188–193

Lönnqvist M, Hökmark H (2016) Thermal, mechanical and thermomechanical assessment of the rock mass surrounding SKB's prototype repository at Äspö HRL. Rock Mech Rock Eng 49(4):1123–1142

Lu YH, Liu QS, Hu YH (2009) Damage deformation characteristics and its strength criterion based on unloading experiments of granites. Chin J Rock Mech Eng 28(10):2096–2103

Nguyen NB, Giraud A, Grgic D (2011) A composite sphere assemblage model for porous oolitic rocks. Int J Rock Mech Min 48(6):909–921

Peng K, Zhou JQ, Zou QL, Zhang J, Wu F (2019a) Effects of stress lower limit during cyclic loading and unloading on deformation characteristics of sandstones. Constr Build Mater 217:202–215

Peng K, Liu ZP, Zhou QL, Zhang ZY, Zhou JQ (2019) Static and dynamic mechanical properties of granite from various burial depths. Rock Mech Rock Eng 1–22

Popov Y, Beardsmore G, Clauser C, Roy S (2016) ISRM suggested methods for determining thermal properties of rocks from laboratory tests at atmospheric pressure. Rock Mech Rock Eng 49(10):4179–4207

Qiu SL, Feng XT, Zhang CZ, Zhou H, Sun F (2010) Experimental research on mechanical properties of deep-buried marble under different unloading rates of confining pressures. Chin J Rock Mech Eng 29(9):1807–1817

Qiu SL, Feng XT, Zhang CZ, Yang JB (2012) Experimental research on mechanical properties of deep marble under different initial damage levels and unloading paths. Chin J. Rock Mech Eng 31(8):1686–1697

Vázquez P, Shushakova V, Gómez-Heras M (2015) Influence of mineralogy on granite decay induced by temperature increase: experimental observations and stress simulation. Eng Geol 189:58–67

Wong TF (1982) Effects of temperature and pressure on failure and post-failure behavior of westerley grinate. Mech Mater 1(1):3–17

Wu G, Zhang L (2004) Studying unloading failure characteristics of a rock mass using disturbed state concept. Int J Rock Mech Min 41(S1):181–187

Xie HQ, He CH (2004) Study of the unloading characteristics of a rock mass using the triaxial test and damage mechanics. Int J Rock Mech Min 41:74–80

Xu XL, Gao F, Zhang ZZ (2014) Research on triaxial compression test of granite after high temperatures. Rock Soil Mech 35(11):3177–3183

Yao MD, Rong G, Zhou CB, Peng J (2016) Effects of thermal damage and confining pressure on the mechanical properties of coarse marble. Rock Mech Rock Eng 49(6):2043–2054

Yin TB, Shu RH, Li XB, Wang P, Liu XL (2016) Comparison of mechanical properties in high temperature and thermal treatment granite. Trans Nonferrous Metal Soc 26(7):1926–1937

Yu QL, Ranjith PG, Liu HY, Yang TH, Tang SB, Tang CA, Yang SQ (2015) A mesostructure-based damage model for thermal cracking analysis and application in granite at elevated temperatures. Rock Mech Rock Eng 48(6):2263–2282

Zhang WQ, Sun Q, Hao SQ, Geng JS, Lv C (2016) Experimental study on the variation of physical and mechanical properties of rock after high temperature treatment. Appl Therm Eng 98:1297–1304

Zhang F, Zhao JJ, Hu DW, Skoczylas F, Shao JF (2018) Laboratory investigation on physical and mechanical properties of granite after heating and water-cooling treatment. Rock Mech Rock Eng 51(3):677–694

Zhu ZN, Tian H, Dong NN, Dou B, Chen J, Zhang Y, Wang BH (2018) Experimental study of physico- mechanical properties of heat-treated granite by water cooling. Rock Soil Mech 39(S2):169–176

Publisher's Note Springer Nature remains neutral with regard to jurisdictional claims in published maps and institutional affiliations.